JOURNAL OF MATERIALS SCIENCE 23 (1988) 1486–1495

Structural inhomogeneity during production and processing of rapidly solidified Al–6Mg–5Fe alloy

E. K. IOANNIDIS, G. J. MARSHALL*, T. SHEPPARD
Department of Materials, Imperial College, London, SW7 2AY, UK

A study of the structural changes occurring during the processing of a rapidly solidified powder aluminium alloy has been performed. Considerable microstructural differences have been noted from among different powder particles and from within the same particle. Three typical microstructures were observed; small particles exhibited a microcellular structure, medium-sized particles a dual morphology of microcellular and cellular structure, whilst in the large particles coarse intermetallics were formed during solidification, acting as nucleation sites for a cellular aluminium structure. Apart from α-Al three other phases were detected in the powder microstructure, Fe_4Al_{13}, (Fe, Mn)Al_6 and an unidentified phase termed "F". The formation of both spheres and needle particles was promoted at high temperatures irrespective of the type of phase (Fe_4Al_{13} or (Fe, Mn)Al_6). It has been shown that the heterogeneity of the microstructural features was maintained during subsequent consolidation via extrusion. The influence of heating and deformation modifies the microstructures but was insufficient to produce a uniform microstructure. The decomposition behaviour of the different microstructures has been examined in detail and the heterogeneities in the extrudate could be related to the powder microstructure and ultimately the solidification behaviour during atomization. The microstructural heterogeneity of the extrudates was characterized by the formation of long bands which normally contained two types of structure. Bands with a high volume fraction of needle-like precipitates and bands with a high volume fraction of spheroids originated from the microcellular and coarser cellular structure, respectively.

1. Introduction

Materials which offer the possibility to achieve superior mechanical properties are under intense development internationally. The requirements for higher strength, higher resistance to corrosion, higher modulus, fatigue and thermal stability stimulated the development of rapid solidification processes. The improved properties resulted firstly from a refined microstructure and secondly from greater chemical homogeneity [1]. Properties were further improved by the use of new alloy compositions through the extension of solute solubility.

The present investigation is an extension of the research at Imperial College, concerning the study of Al–Mg alloys [2, 3]. In general, Al–Mg alloys exhibit medium to high strength, high ductility and high corrosion resistance. However, solid solution strengthening by magnesium in the aluminium matrix, which is the major strengthening mechanism of the binary Al–Mg alloys, does not improve high-temperature strength. Transition elements have been considered to fulfil the requirements for high-temperature strength. These elements exhibit high solubility in molten aluminium but low solid-solubility in aluminium. These qualities together with a low diffusion rate in aluminium are one of the requirements for high temperature strength which is to achieve the microstructural stability by the introduction of a fine dispersion of thermodynamically stable particles. The volume fraction of suitable dispersoid particles is limited in conventionally cast systems of aluminium alloys but may be significantly increased by rapid solidification, because by using the "rapid solidification-powder metallurgy" approach the solid solubility of the transition elements can be considerably increased, e.g. the solubility of iron and manganese from 0.05 wt % and 1.4 wt % to 7.9 to 11.7 wt % and 11.5 to 16.7 wt %, respectively [4]. The effect of transition elements such as chromium, manganese and iron on an Al–7 wt % Mg base alloy has been shown in a preceding publication [3] to improve strength levels and the elastic modulus.

It is important to study the evolution of the microstructure at each stage, from the liquid droplet to the engineering material to ascertain any microstructural changes which may affect product properties. A detailed understanding and explanation of the solidification mechanisms followed by a study of the consolidation procedure are essential to control the parameters affecting the final structure and improve the

* *Present address*: Alcan International, Banbury, Oxfordshire, UK.

0022–2461/88 $03.00 + .12

mechanical properties. In this paper a microstructural study of an Al–6Mg–5Fe R/S alloy is presented as well as a study of the decomposition behaviour of the metastable microstructure during heating and thermomechanical processing, whilst emphasis is placed on any inhomogeneities of the microstructure. In general, rapidly solidified Al–Fe alloys exhibit a variety of microstructures depending upon the cooling rate they have experienced and therefore the size of the rapidly solidified particulates. Jones [5] has observed two zones termed zone A and zone B; Adam [6] reported that P and WA/GPD alloys consist of micro-eutectic and dendritic structures, whilst Boettinger [7] observed four general types of microstructure: micro-cellular, cellular α-Al, fully eutectic α-Al–Al_6Fe and primary intermetallic Al_3Fe structure.

The presence of iron in cast aluminium alloys has a deleterious effect on properties as a result of the relatively coarse intermetallic particles formed. However, the rapid solidification of aluminium iron alloys has been shown to result in very fine dispersions of stable $FeAl_3$ or metastable $FeAl_6$ particles and, therefore, better high-temperature properties than existing commercial high-temperature aluminium alloys [8]. Moreover, the alloy studied in the present work maintains a tensile strength in excess of 550 MPa at ambient temperatures and the elongation to fracture is greater than 4% [3].

2. Experimental procedure

The material was supplied by the Aluminum Company of America in the form of fine powders produced by using an up-draught air atomizer. The chemical composition and size distribution are shown in Table I. The size distribution was conducted by using a Malvern laser particle sizer, whose working principles are based on the scattering of a laser beam which strikes an assembly of particles in suspension. The angle of the diffraction beam is then used to determine the powder particle size.

The study of the powder microstructure was performed using the nickel foil technique, in which nickel foils are impregnated with powder particles; the technique is described in detail elsewhere [2]. Discs of 3 mm diameter were punched from the foil and were mechanically ground to 50 μm thickness. Subsequently the specimens were either electropolished in a solution of 80% ethanol, 10% perchloric acid and 10% 2-butoxyethanol at −30° C or thinned in a Gatan ion-beam thinner. In order to study the evolution of the microstructure and the phase transformations occurring during heating of the powder, cold compacted pads were subsequently hot compacted at 375° C in the extrusion press. Thin slices were then processed to prepare specimens, using the same grinding and electropolishing technique as for consolidated material. The study was performed using a 1000 kV HVEM and a Jeol 120CX transmission electron microscope.

X-ray analysis was performed on the as-received powder, heat-treated powder and consolidated material in order to identify the existing phases and to calculate the lattice parameter of the aluminium matrix. To determine the effect of heating and hence the microstructural stability of the powder, the powder was encapsulated in silicon tubes in an argon atmosphere and heat treated at 50° C intervals in the temperature range from 100 to 500° C. The silicon tubes were water quenched to ensure rapid cooling of the powder.

The diffraction analysis was carried out in a Philips diffractometer using filtered Cu$K\alpha$ radiation. The lattice parameter of aluminium was calculated from the higher order matrix reflections which were plotted against the Nelson–Riley function and an a_0 value obtained by extrapolation.

The powder was cold compacted to billets of approximately 76% density and then rapidly heated in an induction furnace and extruded; details concerning billet preparation and extrusion have been given in a preceding publication [3]. However, a number of partial extrusions has also been performed in order to study the flow properties of the material and the development of the microstructure from powder to a fully dense product. The partial extrusions were terminated during the steady state, just after a peak pressure. The partially extruded billets were then removed from the press and water quenched within approximately 2 min.

Thin foils were prepared firstly from specimens extracted from various positions of the partially extruded billets and secondly from the extrudates using a conventional electropolishing jet technique in a methanol solution of 1.5% HNO_3 and 5% $HClO_4$.

3. Results and discussion

3.1. Powder microstructure

A significant number of powder particles was examined in the transmission electron microscope and typical examples are shown in Figs 1a to c. The structures were observed to be inhomogeneous varying significantly both within individual particles and from particle to particle. Inhomogeneities existing in individual particles are shown in Figs 1a and b. Fig. 1a is a cross-section of a powder particle in which regions of differing microstructure can quite clearly be identified as well as multiple solidification nucleation points resulting in several single nucleation events. Fig. 1b illustrates a particle exhibiting a structural discontinuity of two quite distinct regions. In region A the

TABLE I (a) Powder chemical composition (wt %)

Si	Fe	Mn	Mg	Cr	Ni	Zn	O_2	Al
0.12	5.14	0.80	5.87	0.10	0.01	0.01	0.516	bal.

(b) Size distribution

Size (μm)	+55	−55 + 33.7	−33.7 + 23.7	−23.7 + 17.7	−17.7 + 13.6	−13.6 + 10.5	−10.5
wt %	17.7	28.8	18.5	11.0	6.3	3.5	14.2

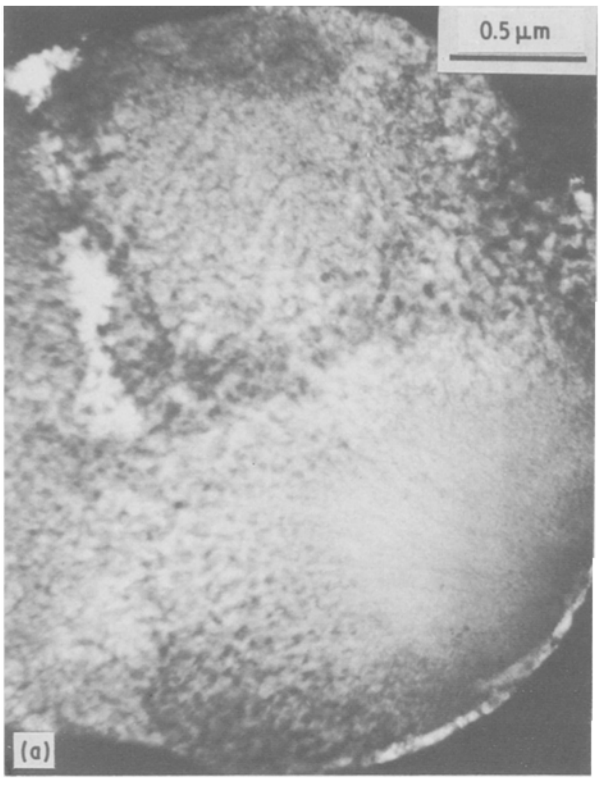

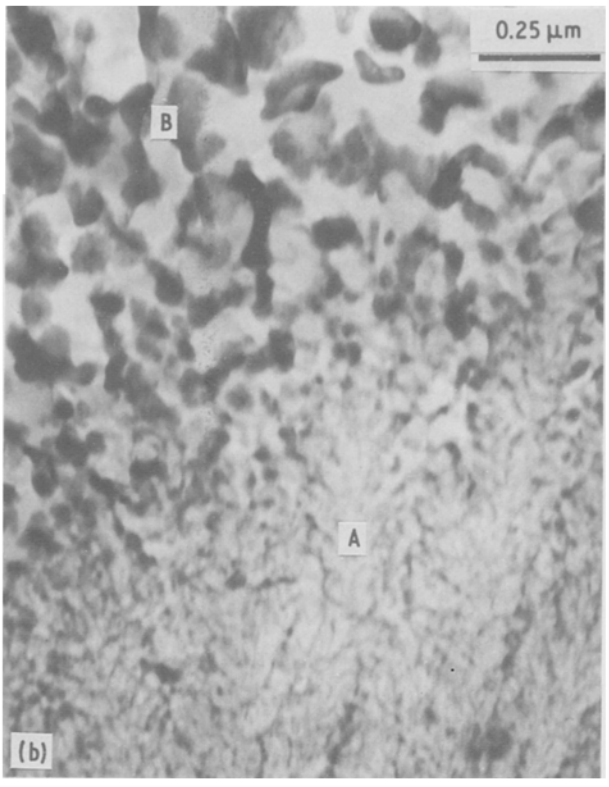

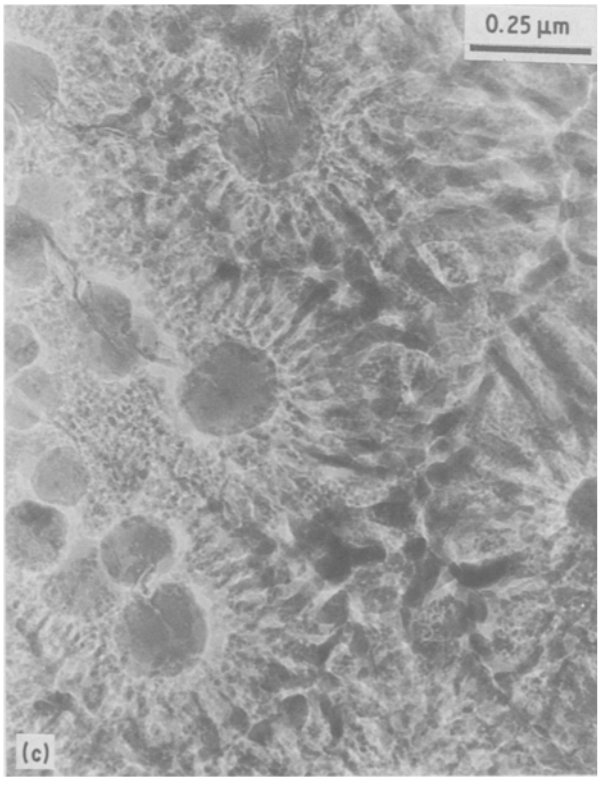

Figure 1 Powder microstructure. (a) Typical cross-section of medium-sized powder. (b) Dual microstructure morphology, microcellular–coarse cellular. (c) Coarse primary intermetallic particles acting as nucleation sites.

structure is extremely fine, designated microcellular, whilst the region marked B has a much coarser cellular morphology. The microcellular structure is one of a uniform cellular network of α-Al solid solution with fine intermetallics at the cell boundaries and it can be seen that, although the transition from microcellular to coarse cellular is relatively abrupt, there is a transition zone over which the cell size gradually increases. Fig. 1c indicates a microstructural characteristic commonly observed in the larger powders in which coarse primary intermetallic spheroids of about 0.2 μm appear to form at commencement of solidification and act as nucleation sites for a fine cellular aluminium matrix which extends radially from the intermetallic.

Theoretical predictions concerning the thermal history of atomized droplets have been published [10–12] but experimental observations of powder microstructures and interpretation of the solidification behaviour to explain the microstructures have been less well reported. The major factors affecting the particle thermal history are the droplet size, nucleation undercooling, heat extraction rate, recalescence and the solid–liquid interface velocity. The solidification model proposed by Levi and Mehrabian [10, 13] suggested two solidification mechanisms; adiabatic and isothermal. In the adiabatic regime a solid–liquid interface velocity advances within an undercooled droplet, accompanied by the release of latent heat whilst the role of the rate of heat extraction to the surroundings is negligible. The amount of solid formed in this regime thus depends upon the size of the particle and the degree of nucleation undercooling. In the isothermal regime, rapid solidification is terminated and the liquid solidifies at a rate determined by heat transfer to the surroundings.

Clearly the powder microstructures observed can be related to the solidification events occurring which are related to the particle size and hence the atomization process. A decrease in the liquid droplet size encourages greater nucleation undercooling and hence the propensity for adiabatic solidification. In the smaller droplets nucleation occurred heterogeneously at the droplet surface and solidification proceeded into the

bulk of the liquid. Large undercooling created the force for a very high velocity solidification front which resulted in the formation of the microcellular structure at a strongly diffusion controlled plane front. As solidification proceeded recalescence occurred due to the release of latent heat and at a rate dependent upon the volume solidified. This reduced the solidification front velocity until below some critical value a cellular front was formed. Completely microcellular structures were typical of the finest powders observed whilst the medium-size powder exhibited a dual morphology; microcellular and cellular. In the large droplets solidification seemed to have been in the isothermal regime; the slower heat extraction rate allowing the formation of randomly distributed solute-rich particles which acted as nucleation sites for any further solidification. Similar coarse morphologies have been reported by Sheppard and Zaidi [14] in an Al–Fe–Mn alloy suggesting that it is the addition of iron which produces these intermetallics. It is certain that magnesium cannot create such particles because powders containing magnesium additions of up to 15 wt % exhibit only cellular morphologies [2].

The microcellular type of structure has been observed in other Al–Fe alloys subjected to high solidification rates [5–7]; the fine microstructure being described by differing terminologies including one instance [6] in which the intercellular structure was reported as amorphous. Clearly the iron addition plays the dominant role during solidification of the Al–Mg–Fe alloy promoting an extremely heterogeneous microstructure.

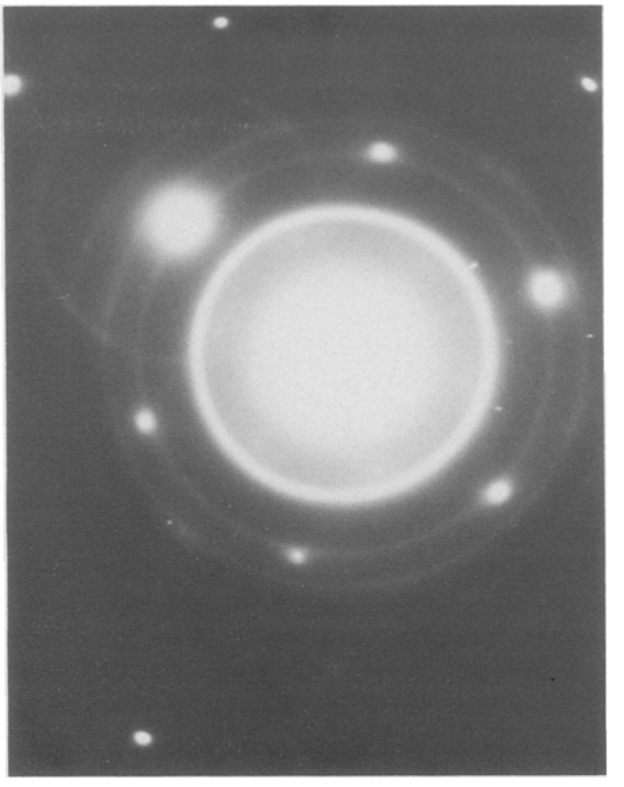

Figure 2 Characteristic electron diffraction pattern from the microcellular type of structure.

3.2. Phase identification

X-ray diffraction analysis revealed three intermetallic phases to be present in the as-atomized powder; equilibrium $Al_{13}Fe_4$ (ASTM 29-42), metastable Al_6–(Fe, Mn) (ASTM 6-0665) and an unidentified phase designated F. The major reflections identified from the analysis are given in Table II which also shows the reported *d*-spacing for $Al_{13}Fe_4$ and Al_6(Fe, Mn). There is no available information in the literature to aid in identifying the "F" phase of this alloy; clearly it must be the result of the iron addition because a

TABLE II Experimentally determined *d*-spacings (nm) and summary of X-ray analysis

Refl. No.	Metastable "F"		Fe_4Al_{13} (ASTM 29-42) [17]		$(Fe, Mn)_6Al$ (ASTM 6-0665) [18]	
	Elect DP	X-ray DP	Reported	Observed	Reported	Observed
1		0.3645	0.2095	0.2097	0.2081	0.2086
2		0.2475	0.2049*		0.2269	0.22681
3		0.2455	0.2041*		0.2153	0.2141
4		0.2227	0.2101	0.2104	0.2027*	
5	0.2120	0.2122	0.2031*		0.1892	0.1890
6	0.1510	0.1513	0.2021*		0.1478	0.1470
7	0.1291	0.1291	0.3545	0.3527	0.4925	0.4901
8	0.1071		0.2015*		0.2621	0.2614
9			0.3962	0.3970	0.2535	0.2522
10			0.4040	0.4040	0.2217	0.2206
11			0.3674	0.3674	0.2187	0.2176
12			0.3268	0.3272		
13			0.2062*			
14			0.4064	0.4058		
Reflections recorded						
Powder						
as received 350° C 1 h	1, 2, 3, 4, 5, 6, 7		1, 4		1, 2, 3	
450° C 1 h	no		1, 4, 7, 9, 10, 11, 12, 14		1, 2, 3, 5, 7, 8, 9, 10, 11	
500° C 1 h	no		1, 4, 7, 9, 10, 11, 12, 14		1, 2 3, 5, 7, 8, 9, 10, 11	
Extrudates						
450° C 20 : 1	no		1, 4, 7, 9, 10, 11, 12, 14		1, 2, 3, 5, 7, 8, 9, 10, 11	
500° C 50 : 1	no		1, 4, 7, 9, 10, 11, 12, 14		1, 2, 3, 5, 7, 8, 9, 10, 11	

*Reflections superimposed on an aluminium pattern.

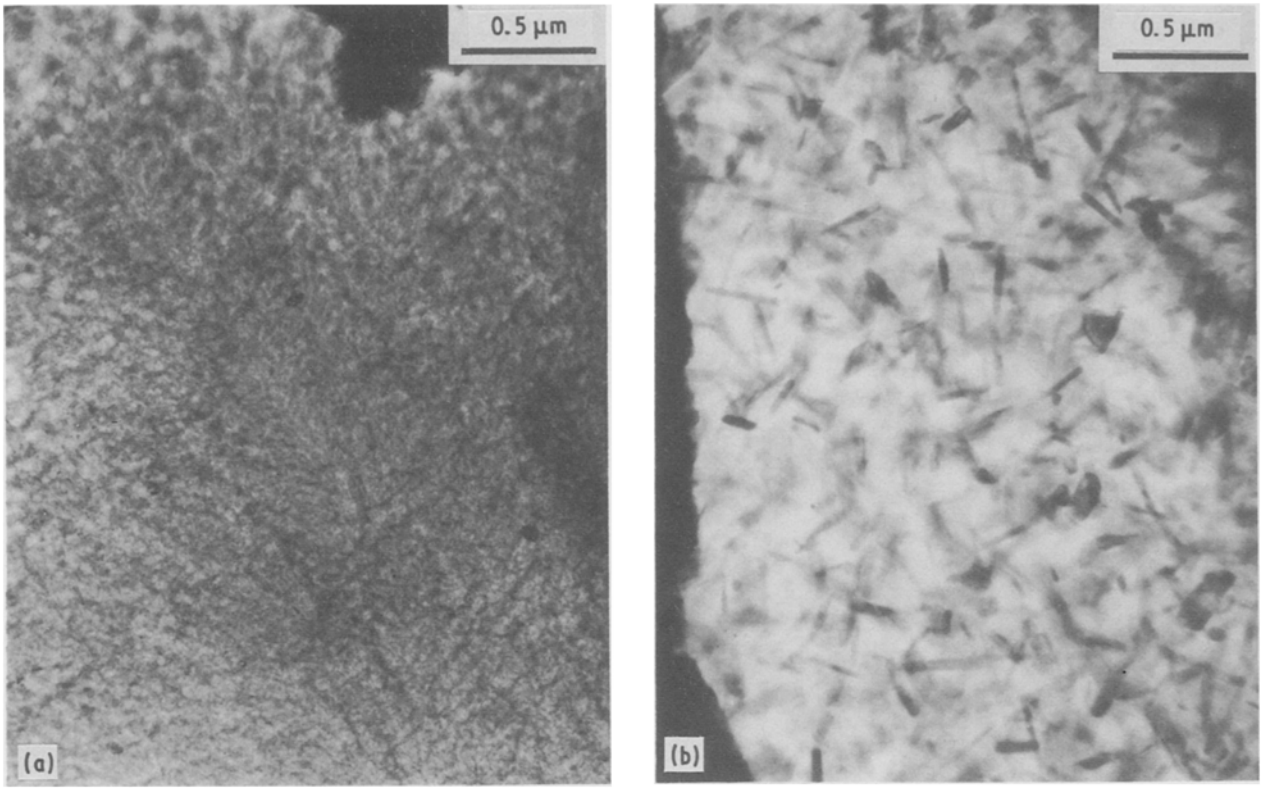

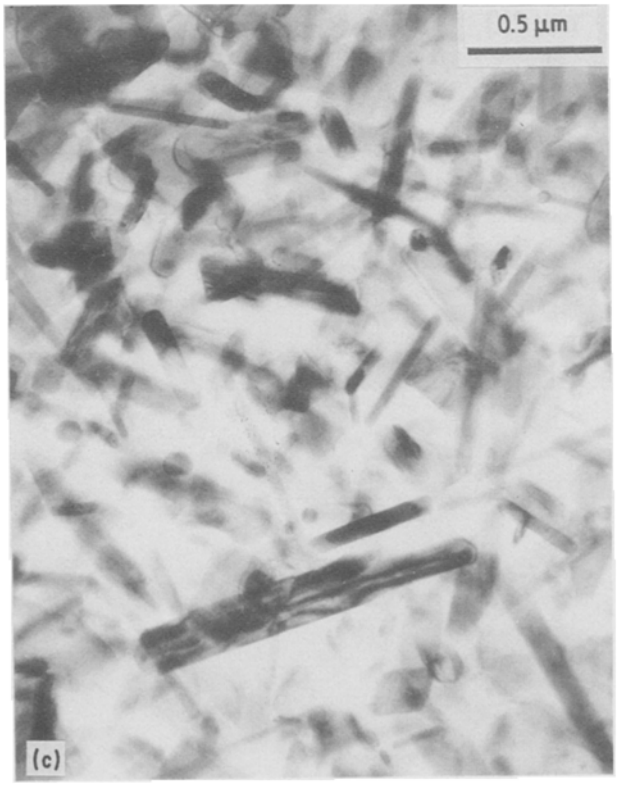

Figure 3 Microstructures from three annealing temperatures: (a) 350° C, (b) 450° C, (c) 550° C.

comprehensive study of the Al–Mg system by Tan [2] did not report the presence of any new phases.

Fig. 2 is an electron diffraction pattern of the microcellular type structure. The ring pattern superimposed on a spot α-Al pattern (zone axis [$\bar{1}$ 1 1]) is consistent with an intercellular network consisting of fine randomly oriented second-phase particles. The reflections of these crystallites correspond to the unidentified "F" phase in the X-ray analysis (Table I). Jacobs *et al.* [15] observed similar fine structures in an Al–8Fe alloy whilst Adam [6] in an analysis of an Al–8Fe–2Mo alloy claimed that the intercellular network was amorphous and of approximate composition Al(Fe, Mo).

Electron diffraction patterns of the intermetallic in the coarser structures could not be obtained because of the greater foil thicknesses required using the nickel substrate technique. However, it seems very probable that these are either Fe_4Al_{13} or (Fe, Mn)Al_6 because the solidification rates experienced by the particles exhibiting coarser structures (i.e. the larger particles) will have been much slower than the particles in which microcellular regions were observed. Identical spheroids have been reported in both coarse and fine structures of Al–8%Fe splats [15].

The reflections from the α-Al were broader and moved towards lower diffraction angles when compared with other rapidly solidified Al–Fe alloys indicating an increase of the lattice parameter of aluminium which must be caused by the magnesium which when in solution expands the lattice of aluminium.

3.3. Heat-treated powder

The consolidation of rapidly solidified powder to produce a fully dense product involves thermomechanical processing which may or may not involve prolonged exposure to high temperatures which is likely to modify the particle microstructure. It is thus important to establish the stability of the phases present in the atomized particles. Representative samples of powder were thus contained in silicon tubes and heated within the hot-working range (350 to 550° C) for 1 h before quenching. It was considered that this time would exceed that experienced by the powder in any practical processing. Figs 3a to c illustrate the structures observed within the hot-working range. At 350° C

there was no apparent change from that observed previously indicating the stability of the alloy at this temperature. X-ray analysis confirmed that the phases remained unchanged and the metastable F-phase untransformed. Increasing the temperature of exposure resulted in considerable changes of microstructure producing a uniform distribution of needle and plate type precipitates as shown in Figs 3b and c. The micrographs shown are representative of most of the powder particles observed and one must conclude that the microstructure is modified by heating. In addition, the metastable "F" phase was transformed; the X-ray results indicate that in powder treated at 450° C only Fe_4Al_{13} and $(FeMn)Al_6$ could be identified.

In situ experiments in the HVEM were performed in order to establish the structural transformations occurring more clearly. The powder for the experiment was compacted to 100% density at 375° C and Fig. 4a shows that this short heat treatment and minimal deformation had little effect on the powder microstructure.

Fig. 4a shows the complete cross-section of a particle exhibiting the dual morphology discussed previously. Region M contains the fine microcellular solidification structure whilst the coarser, post recalescence morphology constitutes region C. This specimen was heated slowly to 400° C (15 min) and held for 90 min whilst the structural changes were observed. During heat-up (Fig. 4b) minor changes to the structure occurred; small discrete precipitates nucleated in region M whilst the coarser structure remained unchanged. After 8 min exposure at 400° C, needle and spherical precipitates formed in both regions although the needle-type precipitates were less pronounced in region C. Thus at this stage the structure is inhomogeneous exhibiting discrete zones of varying structure corresponding to the original morphologies. After 20 min the volume fraction of precipitates increased in each zone (Fig. 4c) and needle-type precipitates could clearly be observed in the coarse morphology region. After 45 min the differing zones still existed but were not as prominent whilst after 90 min the precipitates coarsened throughout the particle, the structure became almost homogeneous and the differing zones were barely distinguishable (Fig. 4d). The transformation is thus gradual with a larger volume fraction of needle-type precipitates being nucleated in the fine microcellular structure but coarsening rapidly during the period 45 to 90 min such that the microstructure is almost homogeneous after 90 min.

3.4. Lattice parameter

Fig. 5 shows the variation of the aluminium lattice parameter with exposure to temperature. In the as-received powder the reflections of α-Al appear at lower diffraction angles to pure aluminium indicating the extension of solid solubility of the alloying elements in the aluminium lattice. The gradual increase of the lattice parameter with temperature (up to 300° C) is consistent with the growth of second-phase particles indicating that manganese and iron precipitate leaving the magnesium in solid solution. At 350° C there is a more significant increase in the aluminium lattice parameter which is a result of the decomposition of the intercellular region and of magnesium being taken into solution. Mondolfo [16] has reported that the lattice parameter of aluminium is practically unchanged by iron contents up to the equilibrium solubility limit (0.05% Fe) but is decreased to 0.04012 nm when 8.4% Fe is retained in solution. Clearly then the increase of the lattice parameter from 0.4071 nm in the atomised powder to 0.4078 nm at 500° C must be a result of redistribution of magnesium.

3.5 Development of structure during extrusion

In this work, the powders were not subjected to a hot pressing and degassing step and hence the extrusion process converted the 76% dense cold compact to a 100% dense engineering material. The microstructural changes occurring within the extrusion chamber were observed by stopping the ram just after peak pressure had been reached and rapidly quenching the partially extruded billet.

Fig. 6 includes a schematic diagram of a billet partially extruded after being heated to 400° C at an extrusion ratio of 20 : 1 and indicates the position from which specimens were extracted from the billet for microscopic examination. The structures of the specimens extracted from the dead metal zone and from the back end of the billet were not dissimilar. The dead metal zone structure is shown in Fig. 6a to consist of tightly packed powder particles clearly defined by the oxide surface film formed during atomization. The particles have been plastically deformed but only sufficiently to ensure their rearrangement into a fully dense structure; the inhomogeneity of the structure generally reflecting that of the initial powder structure. At this location, adjacent particles having very different microstructures were frequently observed. Particle A for example can be seen to consist of coarse dispersoids, particle B has a high volume fraction of needle-shaped precipitates and particle C exhibits a coarse structure with a low volume fraction of precipitates. Inhomogeneities can also be detected on a smaller scale but within the same powder particle; coarse and fine dispersoids can clearly be seen in regions D_1 and D_2 which are not separated by any clearly defined oxide interface. As the particles enter the shear zone they are elongated as shown in Fig. 6b and although the oxide film can still be identified it is ruptured, forming at this juncture, coarse stringers within the material (indicated in Fig. 6b). The needle-shaped precipitates have been aligned in the flow direction and some coarsening of both precipitates and spheroids can be observed. As the material flows through the shear zone the individual particles lose their identity, interparticle bonds are formed and the oxide layer fragmented (Fig. 6c) such that eventually the oxide can no longer be identified (Fig. 6d). Fig. 6d also illustrates the formation of a substructure which at this stage is equiaxed. X-ray analysis revealed three phases to be present in locations such as in Fig. 6c; α-Al, Fe_4Al_{13} and $(Fe, Mn)Al_6$. These reflections from the shear band were sharper indicating that during plastic deformation the kinetics of coarsening is

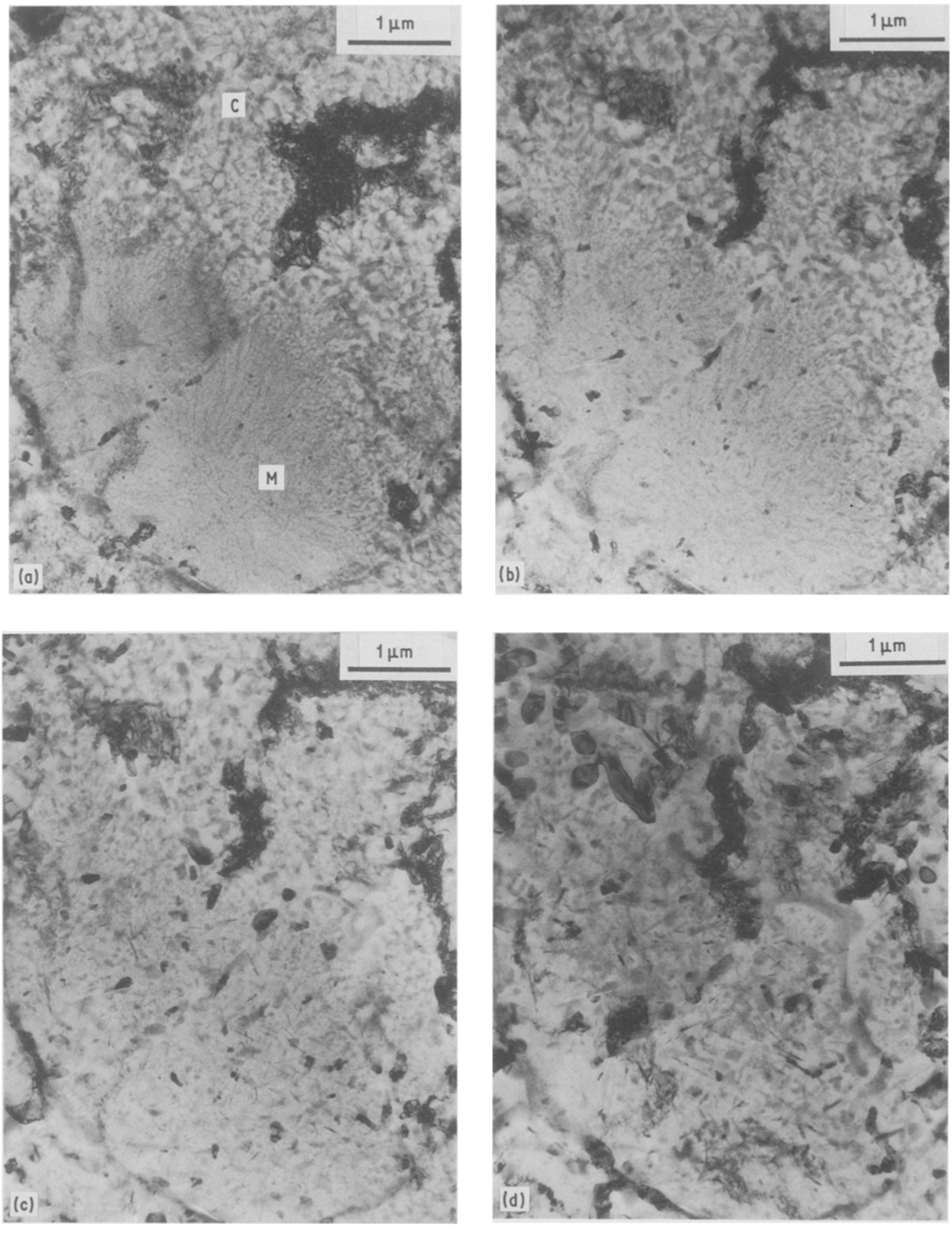

Figure 4 Structural changes during *in situ* heating of hot compacted powder specimens (375° C). (a) Starting microstructure. (b) 400° C, just after the heating up period. (c) 20 min at 400° C. (d) 90 min at 400° C.

considerably enhanced by the imposed shear stresses. The rapid billet heating (5 to 8 min) did not contribute to homogenization of the microstructure, and the dead metal zone gives an indication of powder that has experienced rapid heating and only purely compressive deformation; it is clear that if homogenization is required the powder would require prolonged exposure at elevated temperature. Comparison of the structures in Figs 3, 4 and 6a suggests that the small degree of plastic deformation influences the rate of change due to enhanced atomic mobility and increases in billet temperature. Moreover, by comparing Figs 3, 4 and 6d, the conclusion can be drawn that it would not be possible to reproduce the structures obtained by the superimposed shear and temperature inherent in the extrusion process by any purely thermal processes.

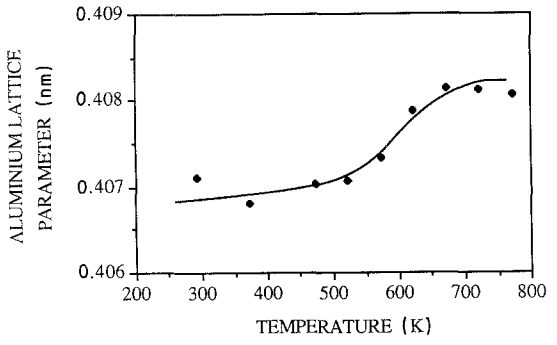

Figure 5 Variation of the lattice parameter of aluminium with heat treatment temperature (1 h duration).

3.6. Extrudate structure

The previous section has indicated that the extrusion process does not remove all of the heterogeneity of the individual atomized powders and hence it is not surprising that the extrudate microstructure was also not homogeneous. The strains imposed upon the powder particles vary for each path through the deformation zone but all are sufficient to ensure that the extrudate exhibits a fibrous structure which is evident in Fig. 7a. Fig. 7a also illustrates the inhomogeneity of the structure where bands of differing structure (presumably from different particles) can be observed aligned in the extrusion direction. In general the original oxide film could not be detected having been fragmented into submicrometre size dispersoids. There was no evidence of oxide stringers which have been reported by other workers [2, 9] but in at least one of these works [9] the oxide content of the powder was significantly higher. Stringers would not then seem to be a particular problem, unless the atomizing conditions are such that high oxide content is produced. This does not presume that oxide dispersoids are not harmful; this has yet to be thoroughly investigated.

The size of both subgrains and dispersoids are a function of the processing condition in which the temperature of extrusion assumes the dominant role. The subgrain size was observed to be heterogeneous at all extrusion temperatures due to the inhibition of dislocation and subgrain boundary motion by the high volume of precipitates distributed throughout the matrix. The microstructural heterogeneity was in general characterized by a banding phenomenon which contained two discrete morphologies. Fig. 7b shows such a band in which a high volume of dispersoids are distributed at sub-grain boundaries; such structures clearly having originated from powder particles with a coarse cellular structure. Bands containing a high volume fraction of needle-type precipitates aligned in the extrusion direction co-existing with spherical dispersoids within the matrix (Fig. 7c) were also a common feature in the extrudate. These latter bands originate from the microcellular structure observed in the powder particles with transformation occurring during the thermomechanical process. The "F" phase was not identified in the processed material in which the dispersoids are precipitates of either Fe_4Al_{13} or $(Fe, Mn)Al_6$.

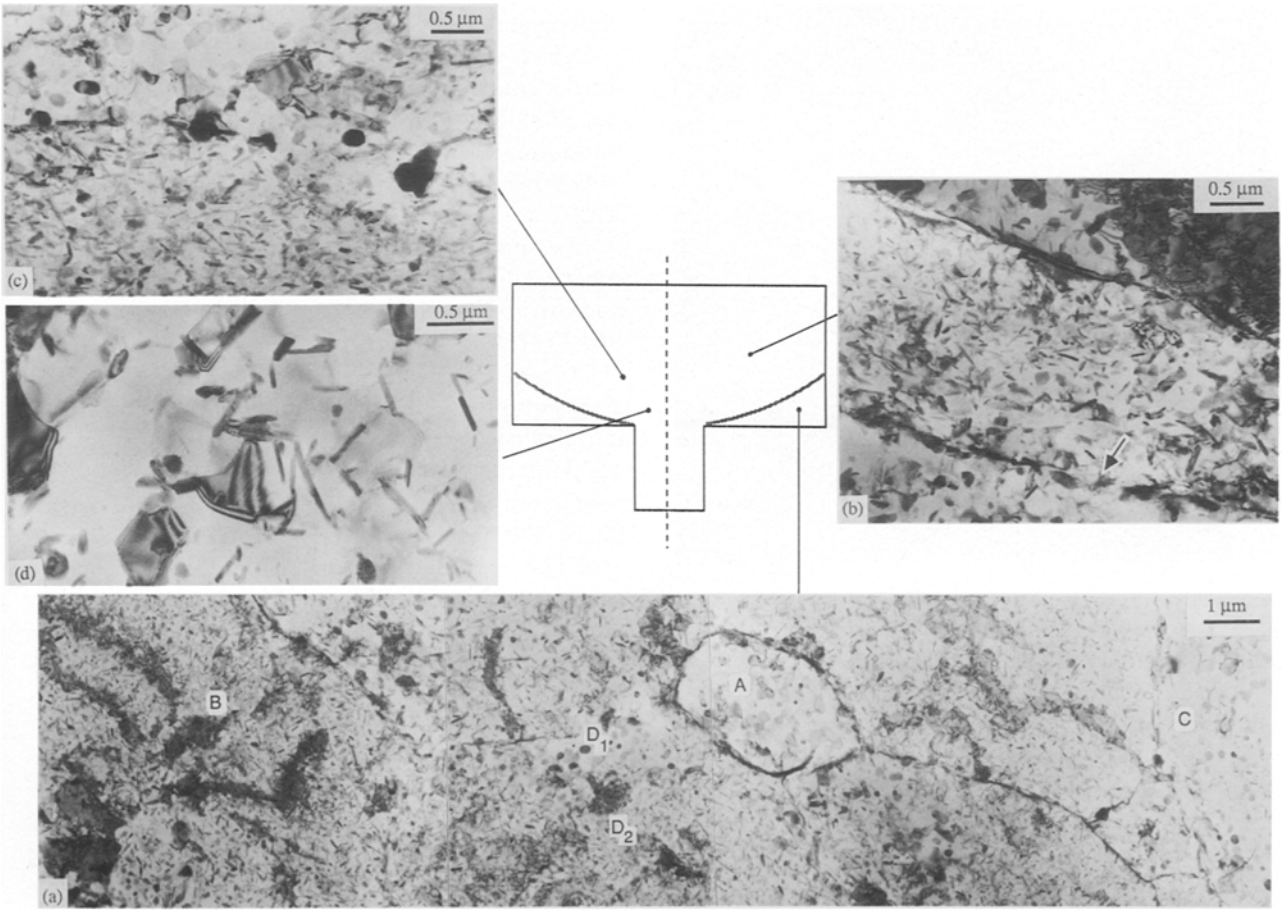

Figure 6 Microstructures from the indicated locations from a partially extruded billet (400° C, 20 : 1) during the steady state.

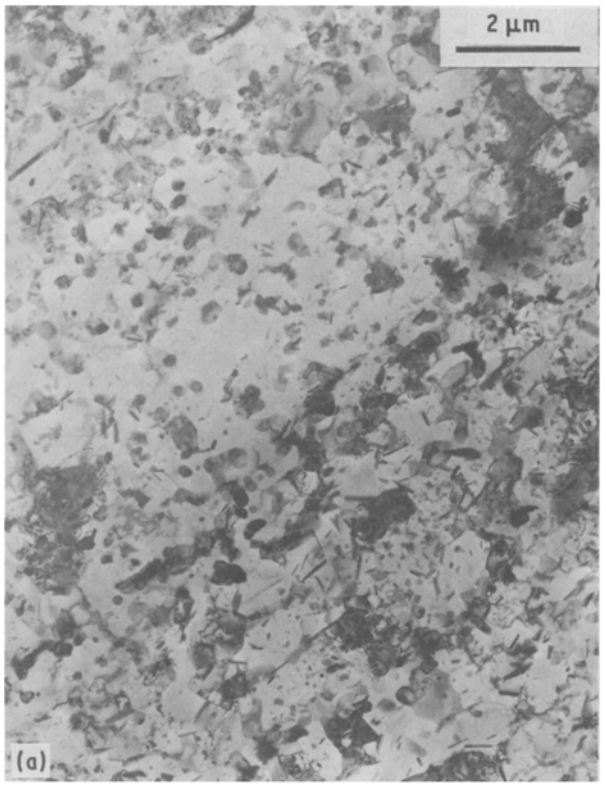

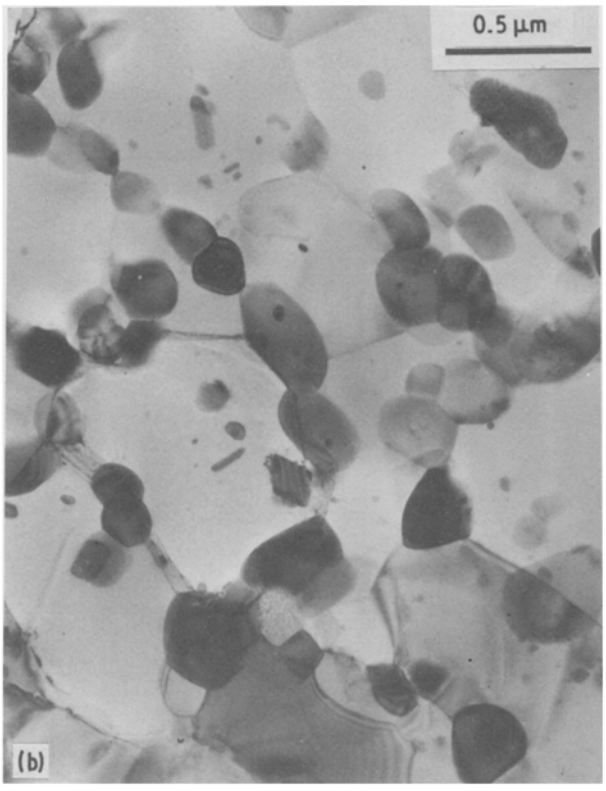

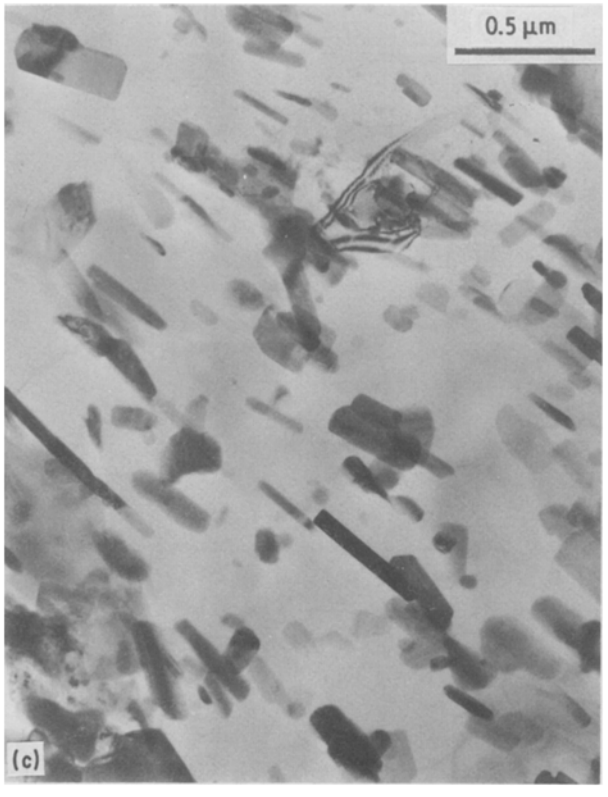

Figure 7 Extrudate microstructure. (a) fibrous extrusion structure. (b) bands with high volume fraction of dispersoids originated from the coarse cellular structure. (c) bands with high volume fraction of needle-shaped precipitates aligned in the extrusion direction, originated from the microcellular type of structure.

4. Conclusions

1. The inhomogeneity observed in the microstructure of the powder particles is an indication of differing solidification behaviour. Small particles exhibit a microcellular structure, medium size a dual morphology which is microcellular and cellular, whilst in the large particles coarse intermetallics formed during solidification, act as nucleation sites for the formation of α-Al cells.

2. Structural variations within the same powder particle have been attributed to different interface velocities caused by the degree of nucleation undercooling and also by recalescence.

3. Two intermetallics, $Al_6(Fe, Mn)$ and $Al_{13}Fe_4$ were identified in the powder particles. An unidentified phase was also observed in the microcellular solidification structure and designated "F".

4. When loose powder is heated temperatures above 400° C are required to coarsen the $Al_6(Fe, Mn)$ and $Al_{13}Fe_4$ phases which then assume either needle or spheroidal morphologies. The initial heterogeneous microstructure is retained until temperatures of about 550° C are encountered.

5. Transformation is much more rapid during the extrusion process when the microcellular transforms into fine needle and spheroidal precipitates whilst the cellular structure transforms to a coarser morphology containing mainly spheroidal precipitates. The "F" phase cannot be identified following extrusion.

6. The extrudate microstructure is also heterogeneous and is related to the powder structure. The structure consists of subgrains of varying size and a non-uniform distribution of spheroidal and needle-type precipitates of $(Fe, Mn)Al_6$ and Fe_4Al_{13}. Frequently banding of dissimilar structures occurs.

Acknowledgements

The financial support of the Bodassakis Foundation, Athens (E.K.I.) and the Department of Trade and Industry (G.J.M.) is gratefully acknowledged. The authors also thank the ALCOA Technical Center (Pittsburgh, USA) for the supply of powder.

References

1. T. E. TIETZ and I. G. PALMER, in "Advances in Powder Technology", (Proceedings of the Conference), Louisville, Kentucky, USA, October 1981 (ASM, Metals Park, Ohio) p. 189–224.
2. G. H. TAN, PhD thesis, University of London (1985).
3. G. J. MARSHALL, E. K. IOANNIDIS and T. SHEPPARD, *Powder Met.* **29** (1986) 57.
4. H. JONES, *Aluminium* **54** (1978) 274.
5. *Idem, Met. Sci. Eng.* **5** (1969/70) 1.
6. C. M. ADAM, in "Rapidly Solidified Amorphous and Crystalline Materials", Proceedings of Materials Research Society Annual Meeting, November 1981, Boston, Massachusetts, edited by B. H. Kear, B. C. Giessen and M. Cohen, Vol. 8 (North Holland, 1982) pp. 411–22.
7. W. J. BOETTINGER, L. BENDERSKY and J. G. EARLY, *Met. Trans. A* **17** (1986) 781.
8. G. THURSFIELD and J. STOWELL, *J. Mater. Sci.* **9** (1974) 1644.
9. T. SHEPPARD, M. A. ZAIDI and G. H. TAN, *Metal Sci.* **17** (1983) 563.
10. C. G. LEVI and R. MEHRABIAN, *Met. Trans. A* **13** (1982) 221.
11. H. JONES, "Rapid Solidification of Metals and Alloys", Monograph No. 8, (Institute of Metallurgists, London, 1982).
12. W. N. GILL, J. W. JANG and J. C. MOLLENDORF, *Chem. Eng. Commun.* **12** (1981) 3.
13. C. G. LEVI and R. MEHRABIAN, *Met. Trans. A* **13** (1982) 13.
14. T. SHEPPARD and M. A. ZAIDI, *Mater. Sci. Technol.* **2** (1986) 69.
15. M. JACOBS, A. DOGGERT and M. STOWELL, *J. Mater. Si.* **9** (1974) 1631.
16. L. F. MONDOLFO, "Aluminium Alloys, Structure and Properties", (Butterworth, London, 1976).
17. P. BLACK, *Acta Crystallogr.* **8** (1955) 43.
18. A. D. I. NICOL, *ibid.* **6** (1953) 285.

Received 24 June
and accepted 22 September 1987